ELSEVIER

Journal of Hydrology 265 (2002) 164–177

Journal of Hydrology

www.elsevier.com/locate/jhydrol

# The use of the aridity index to assess climate change effect on annual runoff

Vivek K. Arora*

*Canadian Centre for Climate Modelling and Analysis, Meteorological Service of Canada, University of Victoria, P.O. Box 1700, Victoria, BC, Canada V8W 2Y2*

Received 15 October 2001; revised 18 March 2002; accepted 3 May 2002

**Abstract**

Available energy (often expressed in terms of potential evaporation) and precipitation largely determine annual evapotranspiration and runoff rates in a region. The ratio of annual potential evaporation to precipitation, referred to as the aridity index by Budyko, has been shown to describe the evaporation ratio (the ratio of annual evapotranspiration to precipitation) of catchments from a range of climatic regimes in a number of studies. It has been shown that aridity index alone can be used to obtain an estimate of ratio of standard deviation of annual evapotranspiration estimates to that of precipitation (the evaporation deviation ratio). At present, there are at least five functional forms available, which describe evaporation ratio as a function of aridity index. This study assesses data from Canadian Centre for Climate Modelling and Analysis' (CCCma) third-generation atmospheric general circulation model (AGCM) against these five functional forms. Evaporation ratio and evaporation deviation ratios from an AGCM simulation are compared against these five functional forms and it is shown that the primary control of available energy and precipitation over annual partitioning of precipitation, and interannual variability of evapotranspiration, is preserved well in the AGCM. The aridity index is further used to obtain an analytic equation, which can be used to estimate change in runoff given annual changes in precipitation and available energy. This equation is validated using data from control and climate change simulations of the CCCma coupled GCM (CGCM1) and shown to perform fairly well. The correlation between CGCM1 simulated annual change in runoff and the values obtained using aridity index is consistently around 0.95, and the average bias varies between 40.5 and 50.3 mm/year, for the five functional forms. The successful validation of this equation against data from a GCM climate change simulation illustrates the continued relevance of aridity index, and the primary control of precipitation and available energy in determining annual evapotranspiration and runoff rates. 

*Keywords:* Climate change; Runoff; Aridity index; General circulation models

## 1. Introduction

For a given region, the annual mean evapotranspiration ($E$) and runoff ($R$) rates are governed primarily by the amount of available energy (the demand) and precipitation ($P$) (the supply). If the available energy and potential evaporation rates are fairly low, then for a given amount of precipitation runoff is likely to exceed evapotranspiration. Similarly, runoff would be expected to be a smaller fraction of precipitation if available radiative energy is very high resulting in high evapotranspiration. The primary control of available energy (i.e. net radiation)

* Fax: +1-250-363-8247.
*E-mail address:* vivek.arora@ec.gc.ca (V.K. Arora).

0022-1694/02/$ - see front matter 
PII: S0022-1694(02)00101-4

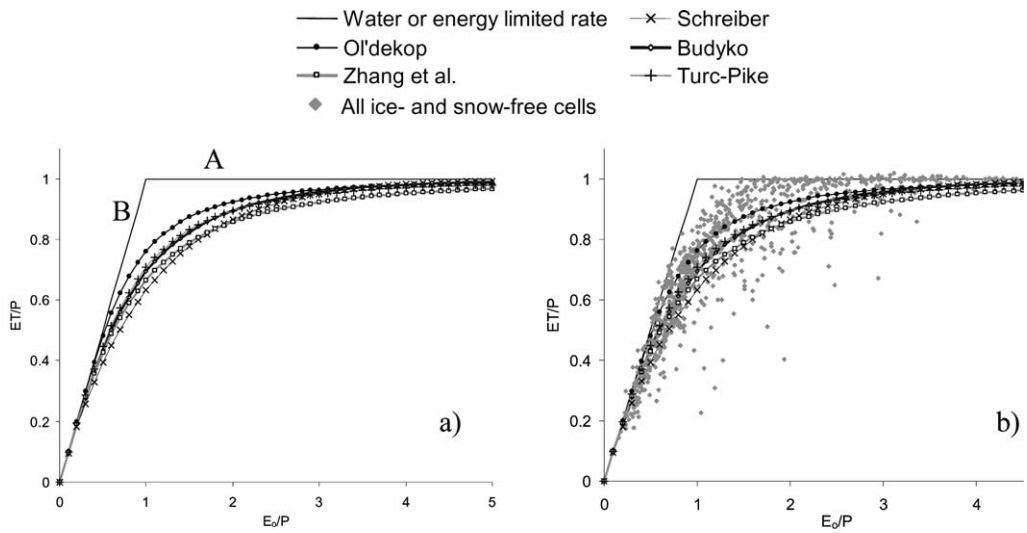


Fig. 1. (a) Comparison of evaporation ratio curves predicted by the Schreiber, Ol'dekop, Budyko, Turc–Pike, and Zhang et al.'s functional forms, and (b) comparison of data from CCCma GCM3 with these five functional forms.

and precipitation in determining annual runoff and evapotranspiration rates has been long recognized. It has been observed that annual evapotranspiration approaches annual precipitation in regions where the available energy greatly exceeds the amount required to evaporate annual precipitation. Conversely, in regions where available energy is a fraction of the amount required to evaporate the entire annual precipitation, the annual evapotranspiration approaches potential evaporation. These two annual evapotranspiration amounts, limited by the available water and energy, are shown as segments A and B, respectively, in Fig. 1a. This figure plots evaporation ratio ($E/P$, the ratio of annual evapotranspiration to precipitation) as a function of the ratio of potential evaporation, $E_0$, to precipitation ($E_0/P$) commonly known as the aridity or dryness index ($\phi$) after Budyko (1974). Regions where aridity index ($\phi$) is greater than unity are broadly classified as dry since the evaporative demand cannot be met by precipitation. Similarly regions with $\phi$ less than unity are broadly classified as wet. The aridity index may also be related to climatic regimes in a broad sense, e.g. arid, semi-arid, sub-humid, and humid regions are defined by the aridity index ranges of $12 > \phi \geq 5$; $5 > \phi \geq 2$; $2 > \phi \geq 0.75$; and $0.75 > \phi \geq 0.375$, respectively (Ponce et al., 2000).

Over an annual time scale the partitioning of precipitation (units of mm) and net radiation ($N$, units of W/m$^2$) into their corresponding water and energy balance components may be written as

$$P = E + R + \Delta S, \tag{1}$$

$$N = LE + H + \Delta G, \tag{2}$$

where $L$ is the latent heat of vaporization, $H$ is the sensible heat flux, $\Delta S$ is the change in moisture storage in soil and snow, and $\Delta G$ is the net ground heat flux. Dividing Eq. (2) by Eq. (1) and assuming $\Delta S$ and $\Delta G$ are small over an annual time scale, $H$ is positive, and representing net radiation ($N$) in terms of potential evaporation ($E_0 = N/L$) yields

$$\frac{E_0}{P} = \frac{E}{P} + \frac{(H/L)}{P}. \tag{3}$$

Representing $H$ in terms of Bowen ratio ($\gamma = H/LE$), the ratio of sensible to latent heat flux, and substituting in Eq. (3) yields

$$\frac{E_0}{P} = \frac{E}{P} + \frac{E\gamma}{P}, \tag{4}$$

which on rearrangement gives an expression for the evaporation ratio ($E/P$) as a function of the aridity

index ($\phi = E_0/P$) and the Bowen ratio ($\gamma$)

$$\frac{E}{P} = \frac{\phi}{1+\gamma}. \tag{5}$$

Eq. (5) is easy to interpret. As a region becomes dry and is characterized by high potential evaporation, low precipitation and evapotranspiration, and high sensible heat fluxes then $\phi \rightarrow \infty$, $\gamma \rightarrow \infty$ and $E/P$ tends towards unity implying little runoff (Fig. 1a). On the other hand, as a region becomes wet and is characterized by low values of aridity index ($\phi$) and Bowen ratio ($\gamma$) then $E/P < 1$ and runoff occurs. Since Bowen ratio ($\gamma$) is also a function of available energy and precipitation (and thus a function of $\phi$) evaporation ratio may be expressed as a function of aridity index alone.

$$\frac{E}{P} = \frac{\phi}{1+f(\phi)} = F(\phi). \tag{6}$$

The assumptions made in deriving Eq. (6) require that the change in moisture storage in soil and snow ($\Delta S$) be small and that sensible heat flux ($H$) be positive. Evaporation ratio for cold regions, which experience permanent ice/snow cover and negative sensible heat flux, therefore, cannot be adequately described in terms of aridity index. Eqs. (5) and (6) form the physical basis of all functional forms which express evaporation ratio as a function of aridity index. For example, Schreiber (1904) developed a simple formula for representing the evaporation ratio as a function of the aridity index in the form

$$\frac{E}{P} = 1 - \mathrm{e}^{-\phi}. \tag{7}$$

The functional form of Schreiber's (1904) relationship implies that the evaporation ratio asymptotically approaches unity for higher values of the aridity index ($\phi$), implying that in extremely arid regions all precipitation is essentially converted into evapotranspiration. Ol'dekop (1911) developed a similar relationship to that of Schreiber (1904) but used a hyperbolic tangent relationship.

$$\frac{E}{P} = \phi \tanh\left(\frac{1}{\phi}\right). \tag{8}$$

Budyko (1948) found that water balance data from a number of catchments, when plotted, lay between the curves proposed by Schreiber (1904) and Ol'dekop (1911). He accordingly proposed the geometric mean of the two relationships.

$$\frac{E}{P} = \left[\phi \tanh\left(\frac{1}{\phi}\right)(1 - \mathrm{e}^{-\phi})\right]^{1/2}. \tag{9}$$

Budyko further tested this relationship for 29 European rivers (Budyko, 1951) and then for 1200 regions for which precipitation and runoff data were available (Budyko and Zubenok, 1961). On the basis of data from 250 catchments from different climatic regimes Turc (1954) proposed a relationship which expressed evaporation ratio as a function of aridity index in the form

$$\frac{E}{P} = \frac{1}{\sqrt{0.9 + \left(\frac{1}{\phi}\right)^2}}. \tag{10}$$

Turc's (1954) relationship was modified by Pike (1964) who found that using 1 instead of 0.9 gave better results. These four functional forms (Schreiber, Ol'dekop, Budyko, and Turc–Pike) numerically behave in a similar manner (Fig. 1a) and the predicted evaporation ratio asymptotically approaches unity for higher values of aridity ratios. Budyko and Turc–Pike curves are hardly distinguishable from each other, and Ol'dekop's curve lies above all curves for values of the aridity index less than about 3. All functional forms deviate from asymptotes A and B, more so around $\phi = 1$, where it appears that there is a transition from energy-limited evapotranspiration (segment B) to water-limited evapotranspiration (segment A). Milly (1994) questioned why transition occurs from B to A and analytically showed that it is the annual cycle of climate which causes this transition. He showed that in absence of an annual cycle, i.e. for constant climate, evapotranspiration is equal to the maximum of $P$ or $E_0$. Indeed, Budyko and Zubenok (1961) noted that when precipitation and potential evaporation have seasonal cycles that are in phase with each other then catchments plot closer to the asymptotes, and when the seasonal cycles of precipitation and potential evaporation are out of phase then catchments plot away from the asymptotes. Asymptotes A and B define the upper water and energy limits to evapotranspiration, and therefore, the minimum runoff for a region. Milly (1994) highlighted other possible causes for deviation from the

asymptotes (i.e. runoff in excess of this minimum). He identifies water-holding capacity of soil, infiltration capacity of soil, and the rate at which the water flows toward plant roots, as three possible causes. For example, if water-holding capacity of the soil is too small then saturation-excess runoff will occur even though aridity index may exceed 1. Precipitation intensities in excess of infiltration capacity will lead to infiltration-excess runoff irrespective of the aridity ratio. Finally, if potential evaporation rates exceed the rates at which water within the root zone can flow short distances to the plant roots (or to bare soil surface), then evapotranspiration may fall short below its water- and energy-limited rates.

In addition to their similar numerical behavior (as shown in Fig. 1a) Eqs. (7)–(10) all assume that the evaporation ratio is principally determined by climatic conditions and the only effect of vegetation on evapotranspiration is through the influence of surface albedo on net radiation. These formulae do not explicitly take into account the effect of type of vegetation and the fact that forests can transpire more water than herbaceous plants and grasses since they have access to potentially larger available water capacity through their deep root systems. Zhang et al. (2001) refer to a number of studies which indicate that deep roots play an important hydrological role in plant systems, especially under dry conditions, and attempt to overcome this limitation by developing a new formula (Eq. (11)). They express evaporation ratio as a function of aridity index ($\phi$) and a plant-available water coefficient ($w$) which in essence attempts to take into account the deviations in evaporation ratio due to variability in water-holding capacity of the soil as pointed by Milly (1994).

$$\frac{E}{P} = \frac{1 + w\phi}{1 + w\phi + \frac{1}{\phi}}. \tag{11}$$

Using data from more than 250 catchments, which varied in area from 1 to $6 \times 10^5$ km$^2$, and in annual rainfall from 35 to 2980 mm, Zhang et al. (2001) estimated the value of plant-available water coefficient ($w$) of 2.0 for catchments dominated by forests, and 0.5 for catchments dominated by short-grass and crops. A higher value of $w$ for forests implies a higher evaporation ratio for a given value of $\phi$. For their relationship, Zhang et al. (2001) found that the plant-available water coefficient ($w$) value of 1.0 provided the best agreement with Schreiber (1904), Budyko (1948), and Pike (1964) relationships.

Budyko (1948) relationship has also been successfully tested using general circulation model (GCM) data by Koster and Suarez (1999) who also developed a relationship, similar to that of Budyko, which expresses the ratio of standard deviation of evapotranspiration to that of precipitation ($\sigma_{ET}/\sigma_P$) as a function of the aridity index.

The successful application of the five functional forms in Eqs. (7)–(11) to observed annual water balance data from catchments around the world, and data from a GCM, emphasize the primary control of precipitation and available energy in determining the ratio of annual evapotranspiration to annual precipitation. This paper assesses the data from Canadian Centre for Climate Modelling and Analysis (CCCma) third-generation atmospheric GCM (AGCM3) against these five functional forms. It assess how the evaporation ratio, and the ratio of standard deviation of annual evapotranspiration to that of precipitation ($\sigma_E/\sigma_P$), from the CCCma AGCM3 compare with those estimated by these five functional forms. The aridity index is further used to obtain an analytic equation, which is used to estimate change in runoff given annual changes in precipitation and potential evaporation. This equation is validated using runoff data from CCCma's first-generation coupled GCM (CGCM1) control and climate change simulations and is shown to perform fairly well.

Section 2 briefly explains the climate model simulations from which the results are used in this study. Analysis of mean annual evapotranspiration and precipitation, and their interannual variability, is presented in Sections 3 and 4, respectively. Section 5 describes the simple analytic equation which is used to obtain an estimate of change in runoff, due to change in climate, and its validation with CGCM1 data. In Section 6, the results of the study are summarized and conclusions are drawn.

## 2. Climate model simulations

Annual evapotranspiration and precipitation data, used to estimate evaporation ratio and the interannual variability of evapotranspiration and precipitation

estimates in Sections 3 and 4, are obtained from the Atmospheric Model Intercomparison Project 2 (AMIP 2) simulation made with the CCCma third-generation atmospheric GCM. CCCma AGCM3 evolved from the CCCma second-generation model (AGCM2) which is described by McFarlane et al. (1992). The results analyzed here are obtained with the T47 32-level version of the model, in which dynamic terms are calculated at triangular T47 spectral truncation, and the physical terms on the associated $96 \times 48$ (3.75°) horizontal linear grid. The vertical domain extends to 1 hPa and the thicknesses of the model's 32 layers increase monotonically with height from approximately 100 m at the surface to 3 km in the lower stratosphere. While many of the parameterized physical processes in the third generation model are qualitatively similar to AGCM2, key new features include: (1) a new parameterization of cumulus convection (Zhang and McFarlane, 1995), (2) an improved treatment of solar radiation which employs 4 bands in the visible and near infrared region, (3) an 'optimal' spectral representation of topography (Holzer, 1996), (4) a revised representation of turbulent transfer coefficients at the surface (Abdella and McFarlane, 1996), (5) a hybrid moisture variable (Boer, 1995), and (6) the introduction of Canadian land surface scheme (CLASS), a new module with three soil layers for treatment of the land surface processes (Verseghy et al., 1993).

In AMIP 2 simulations the atmospheric GCMs are integrated for a 17 year period (1979–1995) with specified lower boundary conditions of observed monthly sea surface temperatures (SST) and sea-ice concentrations (Fiorino, 1997). The AMIP, initiated in 1989 undertook the systematic evaluation, diagnosis, and intercomparison of the performance of the atmospheric GCMs (Gates et al., 1999). For this purpose, participating models simulated the evolution of the climate during the decade 1979–1988. AMIP 2 is an extension of AMIP, with improvements in experimental design, additional diagnosis of an expanded model output and establishment of new standards and protocols for data analysis.

Climate change results used in Section 5 are obtained from the control and transient enhanced greenhouse warming simulations of the CCCma's coupled general circulation model, CGCM1. The climate of CGCM1's control simulation is described by Flato et al. (2000). The atmospheric component of the model is described by McFarlane et al. (1992). It is a spectral model with triangular truncation at wave number 32 (grid resolution roughly $3.7° \times 3.7°$) and 10 levels in the vertical. The ocean component is based on the Geophysical fluid dynamics laboratory (GFDL) MOM1.1 code (Pacanowski et al., 1993) and has a resolution of roughly $1.8° \times 1.8°$ and 29 vertical levels. The model includes a thermodynamic sea-ice component and a single layer bucket soil moisture component whose depth and evapotranspiration rate depend on soil and vegetation type. An ensemble of three transient enhanced greenhouse warming simulations performed with CGCM1 is described by Boer et al. (2000a,b). These simulations follow the IS92a forcing scenario as implemented by Mitchell et al. (1995) where the overall greenhouse gas (GHG) forcing change is specified in terms of an equivalent concentration of $CO_2$. Observational estimates are used from 1850 to the present. Thereafter, an increase of $CO_2$ at a rate of 1% per year (compounded) until the year 2100 is imposed. The direct forcing effect of sulphate aerosols is also included by increasing the surface albedo (Reader and Boer, 1998) based on results from the sulphur cycle model of Langner and Rodhe (1991).

## 3. Analysis of mean annual evapotranspiration and precipitation

Mean annual evapotranspiration and precipitation estimates from the 17 year AMIP 2 simulation made with CCCma AGCM3 are used to obtain the evaporation ratio. Potential evaporation, $E_0$, values are obtained as

$$E_0 = \frac{N}{L}, \tag{12}$$

where $N$ is the net radiation and $L$ is the latent heat of vaporization. The use of net radiation in this context is to represent the maximum evapotranspiration that could occur for given climatic conditions. Values of potential evaporation in this study are easily obtained using net radiation from the GCM since the land surface scheme takes into accounts the energy balance. In practice, however, estimation of potential evaporation could be a large source of error. Budyko

(1974) himself used net radiation instead of potential evaporation and argued that the upper limit for evapotranspiration is equal to net radiation. Grid cells with year-round ice and snow cover are not considered, (1) because these cells have a potential for long-term moisture storage in form of snow/ice and this violates the assumption that precipitation be balanced by evapotranspiration and runoff, and (2) because many of these grid cells are characterized by negative sensible heat fluxes which allows mean annual evapotranspiration, ET, to exceed potential evaporation, $E_0$.

Evaporation ratio obtained using GCM data, for 869 ice- and snow-free grid cells, is plotted against the aridity index in Fig. 1b. The GCM points are overlaid by the curves predicted by the five functional forms. Grid cells (78 in number) with aridity index more than 5 are not shown in the figure although their evaporation ratio, as expected, is found to be close to 1. The GCM data show a clear increase in evaporation ratio ($E/P$) with an increase in the aridity index ($\phi$) and the qualitative shape of the GCM data compare well with the five functional forms. The correlation between model evaporation ratio and that predicted by these five functional forms varies between 0.925 and 0.934. There is substantial scatter around the curves. This is expected since these functional forms do not take into account (1) the annual cycles of precipitation and potential evaporation and if they are in or out of phase, (2) that surface runoff can be generated due to saturation- and infiltration-excess, and (3) that transpiration from vegetation may not occur at a rate determined by the aridity index. Nevertheless, the relationship between evaporation ratio and the aridity index is strong enough to illustrate that a reasonable first-order estimate of evaporation ratio can be obtained from aridity index. The fair agreement between GCM results and the five functional forms affirms that the primary control of precipitation and available energy in annual partitioning of precipitation into evapotranspiration and runoff is preserved reasonably well in the GCM.

This, however, is by no means a test of GCM annual precipitation, evapotranspiration, and runoff fluxes against observations. Precipitation and runoff estimates from CCCma GCM3 are compared with observations in Arora and Boer (2002) and Arora (2001a,b) who find that although the globally averaged precipitation and runoff over land are simulated well in the model there remain discrepancies in regional estimates of these quantities.

## 4. Analysis of interannual variability

Koster and Suarez (1999) extend the use of aridity index to predict interannual variability of the evapotranspiration and runoff fluxes. Assuming interannual changes in soil moisture storage ($\Delta S$) are much smaller than the annual precipitation, evapotranspiration, and runoff fluxes, they write evaporation ratio for $i^{\text{th}}$ year as a function of that year's aridity index,

$$\frac{E_i}{P_i} = F(\phi_i), \qquad \phi_i = \frac{E_{0_i}}{P_i}. \tag{13}$$

Using Eq. (13), the deviation of the $i^{\text{th}}$ year evapotranspiration ($\Delta E_i$) can be written in terms of deviation of precipitation ($\Delta P_i$), and aridity index ($\Delta\phi_i$) from their respective climatological means as

$$\Delta E_i = F(\phi)\Delta P_i + PF'(\phi)\Delta\phi_i. \tag{14}$$

Expanding $\Delta\phi_i$ in terms of $\Delta P_i$ and $\Delta E_{0_i}$

$$\Delta\phi = \frac{\Delta E_0}{P} - \frac{E_0}{P^2}\Delta P$$

and substituting in Eq. (14) yields

$$\Delta E_i = [F(\phi) - \phi F'(\phi)]\Delta P_i + F'(\phi)\Delta E_{0_i}. \tag{15}$$

Squaring, time-averaging, and re-arranging Eq. (15) yields an expression for 'evaporation deviation ratio', that is the ratio of standard deviation of annual evapotranspiation to that of annual precipitation.

$$\left(\frac{\sigma_E}{\sigma_P}\right)^2 = [F(\phi) - \phi F'(\phi)]^2 + F'(\phi)^2\left(\frac{\sigma_{E_0}}{\sigma_P}\right)^2 + 2[F(\phi) - \phi F'(\phi)]F'(\phi)\frac{\mathrm{cov}(P, E_0)}{\sigma_P^2}. \tag{16}$$

Eq. (16) implies that evaporation deviation ratio is a function of aridity index, the mathematical form of $F(\phi)$, and deviations in precipitation and potential evaporation from their climatological means. Under the assumption that interannual variations in net radiation (and thus potential evaporation) are generally smaller than those of precipitation, Koster and

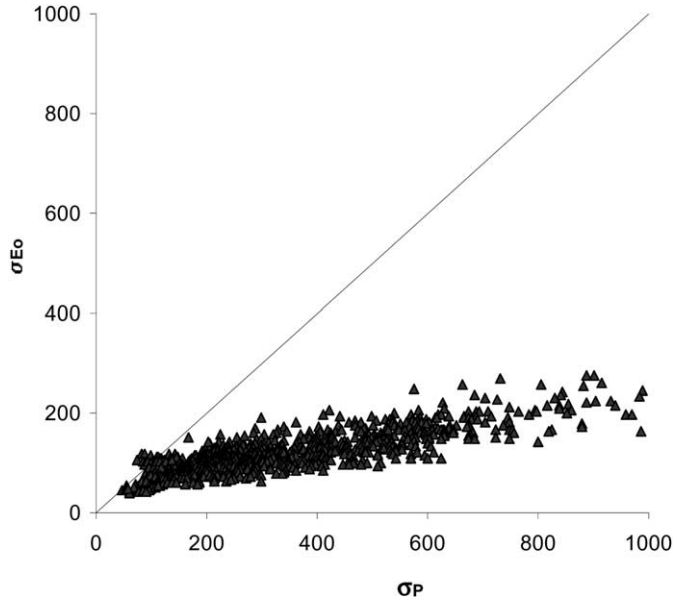


Fig. 2. Standard deviation of model annual potential evaporation estimates ($\sigma_{E_0}$) plotted against the standard deviation of model precipitation estimates ($\sigma_P$). The 1:1 line is also shown.

Table 1
Mathematical expressions for evaporation deviation ratio ($\sigma_E/\sigma_P$) for all five functional forms

| Functional form | $\frac{\sigma_E}{\sigma_P} = F(\phi) - \phi F'(\phi)$ |
|---|---|
| Schreiber | $\frac{\sigma_E}{\sigma_P} = 1 - e^{-\phi} - \phi e^{-\phi}$ |
| Ol'dekop | $\frac{\sigma_E}{\sigma_P} = \frac{4}{\left(e^{1/\phi} + e^{-1/\phi}\right)^2}$ |
| Budyko | $\frac{\sigma_E}{\sigma_P} = \frac{\phi \tanh\left(\frac{1}{\phi}\right)[1 - e^{-\phi} - \phi e^{-\phi}] + \mathrm{sech}^2\left(\frac{1}{\phi}\right)[1 - e^{-\phi}]}{2\left[\phi \tanh\left(\frac{1}{\phi}\right)(1 - e^{-\phi})\right]^{1/2}}$ |
| Turc–Pike | $\frac{\sigma_E}{\sigma_P} = \frac{1}{\left[1 + \left(\frac{1}{\phi}\right)^2\right]^{1/2}} - \frac{1}{\phi^2\left[1 + \left(\frac{1}{\phi}\right)^2\right]^{3/2}}$ |
| Zhang et al. | $\frac{\sigma_E}{\sigma_P} = \frac{1 - w + \phi + w\phi(1 + w\phi)}{\left(1 + w\phi + \frac{1}{\phi}\right)^2}$; $\quad \frac{\sigma_E}{\sigma_P} = \frac{2\phi + \phi^2}{\left(1 + \phi + \frac{1}{\phi}\right)^2}$, for $w = 1$ |

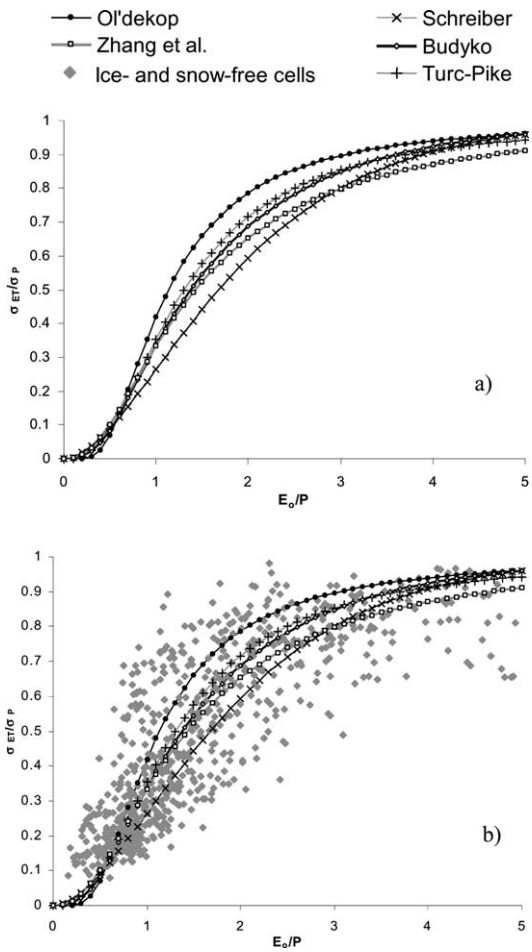


Fig. 3. (a) Comparison of evaporation deviation ratio curves predicted by the Schreiber, Ol'dekop, Budyko, Turc–Pike, and Zhang et al.'s functional forms, and (b) comparison of evaporation deviation ratio from CCCma AGCM3 with these five functional forms.

Suarez (1999) write Eq. (16) in a simplified form as

$$\frac{\sigma_E}{\sigma_P} = F(\phi) - \phi F'(\phi). \quad (17)$$

Using data from a GCM, they show that standard deviation of net radiation is generally, but not universally, smaller than standard deviation of precipitation. Fig. 2 shows the standard deviation of annual potential evaporation estimates ($\sigma_{E_0}$) plotted against the standard deviation of precipitation estimates ($\sigma_P$) using data from the AMIP 2 simulation of the CCCma AGCM3 for 869 ice- and snow-free grid cells. The assumption that $\sigma_{E_0}$ is generally less than $\sigma_P$ is true for most land cells. A few land cells, however, do lie above and extremely close to the 1:1 line in Fig. 2. At these points, where $\sigma_P$ is small, interannual variations in potential evaporation and precipitation are of similar magnitude.

Using Eq. (17), the Schreiber, Ol'dekop, Budyko, Turc–Pike, and Zhang et al.'s functional forms are used to obtain their corresponding expressions for predicting evaporation deviation ratio $\sigma_E/\sigma_P$ and these are shown in Table 1. The expression for evaporation deviation ratio for Budyko's functional form is same as that obtained by Koster and Suarez (1999) and a value of $w = 1$ is used for Zhang et al.'s (2001) functional form, i.e. when no distinction is made between forested and herbaceous catchments. The curves for evaporation deviation ratio predicted by these five functional forms are compared in Fig. 3a. As expected, despite their different mathematical forms, the qualitative shapes of the $\sigma_E/\sigma_P$ versus $\phi$ curves predicted by the five functional forms are fairly similar. Evaporation deviation ratio $\sigma_E/\sigma_P$ obtained from the AMIP 2 simulation is plotted against the aridity index ($\phi$), and overlaid $\sigma_E/\sigma_P$ versus $\phi$ curves predicted by the five functional forms, in Fig. 3b. About 110 grid cells (out of 869) at which variations in potential evaporation were significant ($\sigma_{E_0}/\sigma_P > 0.6$) are excluded. These points are excluded since at these points evaporation deviation ratio also depends on interannual variations of potential evaporation (which are of similar magnitude to interannual variations in precipitation) and therefore, at these points Eq. (17) is not a good approximation of Eq. (16). The first-order relationship between $\sigma_E/\sigma_P$ and $\phi$ agrees well with the curves predicted by the five functional forms. The correlation between model evaporation deviation ratio and that predicted by these five functional forms varies between 0.840 and 0.854.

Fig. 3a and b show that as the aridity index increases (and the climate becomes drier) the magnitude of the interannual variations in evapotranspiration tends to become as large as the magnitude of interannual variations in precipitation. For extremely wet regions, characterized by smaller values of aridity index ($\phi < 1$), the interannual variations in evapotranspiration are small (relative to precipitation) since evapotranspiration in wet regions is controlled by available energy which generally shows little variation from year to year relative to precipitation (Fig.

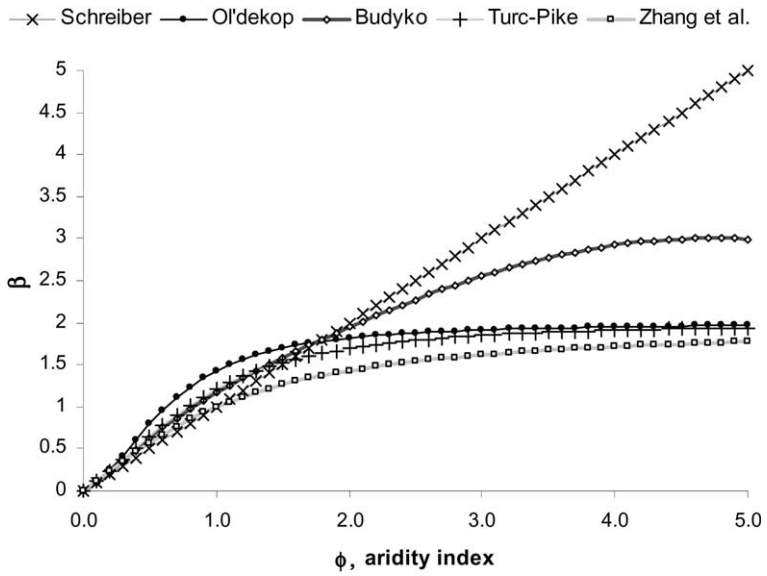


Fig. 4. The sensitivity factor $\beta$ plotted against the aridity index $\phi$ for the five functional forms.

2). Conversely, in arid regions ($\phi > 4.5$) since nearly all precipitation is converted into evapotranspiration, the interannual variations in evapotranspiration and precipitation are of similar magnitude. There is substantial scatter in Fig. 3b and this is the result of (1) assuming that interannual changes in moisture storage are small, (2) neglecting interannual variations in precipitation and potential evaporation (i.e. the last two RHS terms in Eq. (16) are ignored), and (3) the small 17-year duration of the AMIP 2 simulation. Scatter in Fig. 3b is also the result of neglecting infiltration- and saturation-excess runoff and the phasing of precipitation and potential evaporation annual cycles in estimating annual runoff. Nevertheless, the $\sigma_E/\sigma_P$ versus $\phi$ curves predicted by the five functional forms describe the first-order dependence of interannual variations in evapotranspiration on aridity index reasonably well.

## 5. Use of aridity index to estimate change in runoff

The use of aridity index is extended to obtain an estimate of change in annual runoff, due to a change in climate, given information about changes in annual precipitation and potential evaporation. A change in climate may cause either or both precipitation and potential evaporation to change. A change in potential evaporation may be due to (1) a change in temperature (e.g. due to climate warming), (2) a change in net radiation associated with a change in albedo (e.g. due to land-use change), or (3) both.

Following Eq. (15), and omitting the subscript $i$ for clarity, the change in runoff due to change in precipitation and potential evaporation is given by

$$\Delta R = \Delta P - \Delta E$$
$$\Delta R = \Delta P[1 - F(\phi) + \phi F'(\phi)] - \Delta E_0 F'(\phi). \tag{18}$$

Change in runoff can also be expressed as a fraction of original runoff [$R = P(1 - F(\phi))$]

$$\frac{\Delta R}{R} = \frac{\Delta P[1 - F(\phi) + \phi F'(\phi)] - \Delta E_0 F'(\phi)}{P[1 - F(\phi)]}, \tag{19}$$

which on rearranging yields

$$\frac{\Delta R}{R} = \frac{\Delta P}{P}(1 + \beta) - \frac{\Delta E_0}{E_0}\beta, \tag{20}$$

where

$$\beta = \frac{\phi F'(\phi)}{1 - F(\phi)}. \tag{21}$$

Eq. (20) implies that the fractional change in annual runoff is a function of fractional changes in annual

Table 2
Mathematical expressions for $F'(\phi)$ for all five functional forms

| Functional form | $F'(\phi)$ |
|---|---|
| Schreiber | $F'(\phi) = e^{-\phi}$ |
| Ol'dekop | $F'(\phi) = \tanh\left(\frac{1}{\phi}\right) - \frac{4}{[\phi(e^{-1/\phi} + e^{1/\phi})^2]}$ |
| Budyko | $F'(\phi) = \frac{1}{2}\left[\phi \tanh\left(\frac{1}{\phi}\right)(1 - e^{-\phi})\right]^{-1/2}\left[\left(\tanh\left(\frac{1}{\phi}\right) - \frac{1}{\phi}\mathrm{sech}^2\left(\frac{1}{\phi}\right)\right)(1 - e^{-\phi}) + \phi \tanh\left(\frac{1}{\phi}\right)e^{-\phi}\right]$ |
| Turc–Pike | $F'(\phi) = \frac{1}{\phi^3\left[1 + \left(\frac{1}{\phi}\right)^2\right]^{3/2}}$ |
| Zhang et al. | $F'(\phi) = \frac{w + \frac{2w}{\phi} - 1 + \frac{1}{\phi^2}}{\left(1 + w\phi + \frac{1}{\phi}\right)^2}$; $F'(\phi) = \frac{\frac{2}{\phi} + \frac{1}{\phi^2}}{\left(1 + \phi + \frac{1}{\phi}\right)^2}$, for $w = 1$ |

precipitation and potential evaporation, and the value of the coefficient $\beta$ (which depends on the aridity index, $\phi$). Eq. (20) is similar to the one obtained by Dooge (1992) and Dooge et al. (1999) who express their formulae in terms of the humidity index ($1/\phi$) rather than the aridity index. The mathematical form of Eq. (20) and the functional form of coefficient $\beta$ obtained here are, therefore, different from Dooge (1992) and Dooge et al. (1999). Eq. (20) is easy to interpret. In the absence of any change in potential evaporation ($\Delta E_0 = 0$) change in runoff is solely determined by change in precipitation. Conversely, in the absence of change in precipitation ($\Delta P = 0$), change in potential evaporation governs the change in runoff. When change in potential evaporation is associated with a change in precipitation then their absolute magnitudes determine the change in runoff.

The coefficient $\beta$ may be considered as a sensitivity index in a broad sense. If only one of precipitation or potential evaporation changes, then a larger value of $\beta$ implies a larger change in runoff. Fig. 4 shows the coefficient $\beta$ plotted as a function of the aridity index ($\phi$) for the five functional forms considered in this study and the $F'(\phi)$ expressions used to obtain $\beta$, for the five functional forms, are summarized in Table 2. The value of coefficient $\beta$ increases as the aridity index increases, and this implies that runoff is more sensitive in dry and arid regions. Dooge (1992) draws a similar conclusion although the functional form of his sensitivity index is different and based on the humidity index. When changes in potential evaporation are associated with changes in precipitation, then it is the absolute magnitudes of these quantities that determine the change in runoff and the effect of $\beta$ in determining the change in runoff may not be obvious. In Fig. 4, Schreiber's formulation stands out and predicts that $\beta$ continues to increase with aridity index while all other formulations predict that for larger values of the aridity index the coefficient $\beta$ becomes relatively constant. This is a numerical artifact of Schreiber's formulation.

### 5.1. Test of the climate change equation

While Dooge (1992) and Dooge et al. (1999) use an expression similar to Eq. (20) to explore the sensitivity of runoff, to change in climate, in various climatic regimes they do not explicitly attempt to validate their expression. In this study, data from the

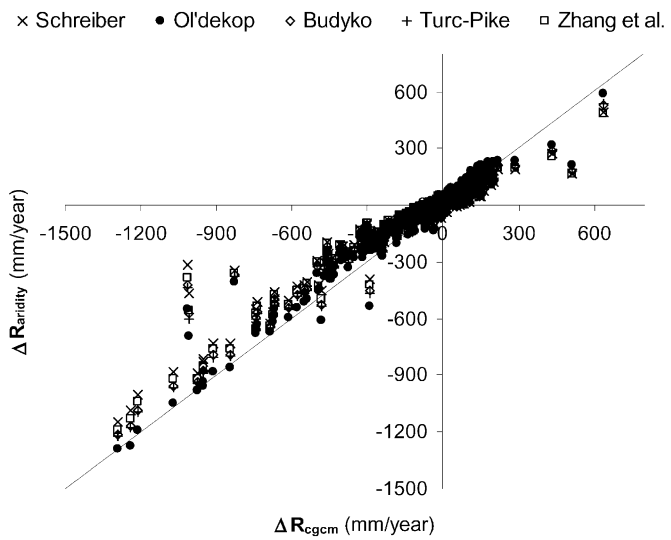


Fig. 5. Comparison of change in runoff estimated by Eq. (20) ($\Delta R_{\text{aridity}}$) with values obtained from CCCma's coupled GCM ($\Delta R_{\text{cgcm}}$). The 1:1 line is also shown.

control and transient enhanced greenhouse warming simulations of CCCma's first-generation coupled general circulation model (CGCM1) are used to test Eq. (20). As mentioned in Section 2, the CGCM1 uses the bucket soil moisture component that treats the land surface processes in a much simpler manner than the CLASS land surface scheme used in AGCM3. Thirty-one years of annual precipitation, potential evaporation, and runoff data from the years 1965–1995 of the control simulation and years 2070–2100 of the transient GHG simulation of CGCM1 are used to estimate mean annual values. As mentioned in Section 3, the potential evaporation estimates are obtained using model's net radiation data. The mean annual values of precipitation and potential evaporation from the control simulation are then used to estimate aridity index ($\phi$) for all ice- and snow-free grid cells. The changes in precipitation ($\Delta P$) and potential evaporation ($\Delta E_0$) are obtained from the difference between values from the control and GHG simulations, and these are used in Eq. (20) together with aridity index to estimate predicted change in runoff ($\Delta R_{\text{aridity}}$).

Changes in runoff predicted using aridity index, $\Delta R_{\text{aridity}}$, (using Eq. (20)) are compared with CGCM1 simulated changes, $\Delta R_{\text{cgcm}}$, in Fig. 5. Eq. (20) predicts the change in annual runoff, given the changes in precipitation and potential evaporation, reasonably well. The correlation between CGCM1 and values predicted by Eq. (20) varies between 0.948 and 0.953 for the five functional forms. The average bias

$$\left(\sum_{1}^{n} |\Delta R_{\text{cgcm}} - \Delta R_{\text{aridity}}|/n\right)$$

in values predicted using Eq. (20) varies between 40.5 (Ol'dekop) and 50.3 (Schreiber) mm/year. The small bias and the high correlation between CGCM1 and Eq. (20) values demonstrates the continued relevance of aridity index in analyses of Budyko and other researchers. It is also interesting to note that the $\Delta R_{\text{aridity}}$ values predicted by the five functional forms are fairly similar to each other and no single functional form stands out as an outlier. Thus any of the five functional forms may be used to obtain an estimate of change in runoff. Note that the scatter present in Fig. 1b (when predicting evaporation ratio) and Fig. 3b (when predicting evaporation deviation ratio) using aridity index is significantly reduced in Fig. 5. There are two possible reasons for this. First, the bucket land surface scheme used in CGCM1 does not account for runoff generation due to infiltration-excess, and saturation-excess runoff only occurs when the entire bucket becomes saturated (which is not expected to occur often, especially since precipitation intensity is assumed to be uniformly distributed over

the large GCM grid cells). The absence of infiltration- and saturation-excess runoff brings the bucket model closer to the model of Budyko and other researchers. However, since the coupled GCM itself is run at a time step of few minutes the bucket model does not ignore the annual cycles of precipitation and potential evaporation. Second, and the more likely reason is that, since the quantity being evaluated is the change in runoff ($\Delta R$) and not the absolute runoff, the errors that might result due to neglect of runoff generation mechanisms and consideration of annual cycle of precipitation and potential evaporation in the five functional forms, are cancelled out.

Most grid cells in Fig. 5 are plotted with negative $\Delta R$ values since CGCM1 simulates a decrease in globally averaged runoff by 14% due to climate warming (Arora and Boer, 2000). Using the same data as in this study, Arora and Boer (2001) analyze results from CGCM1 for 23 major river basins and show that the model simulates a median decrease of 32% in mean annual discharge for 15 out of 23 major river basins considered. For the remaining 8 rivers the median increase in mean annual discharge is found to be 13%.

The estimates of change in precipitation and potential evaporation for use in Eq. (20) can be obtained from GCM and/or regional climate model (RCM) simulations. These values may also be assumed arbitrarily to perform sensitivity studies as is done in a number of hydrological studies (Nemec and Schaake, 1982; Chiew et al., 1995; Avila et al., 1996; Singh and Kumar, 1997). Eq. (20) may thus be used to obtain a first-order estimate of change in annual runoff based on changes in precipitation and potential evaporation in a fairly straight-forward manner without performing any detailed hydrological model simulations. The successful validation of Eq. (20) against GCM data re-emphasizes the control of annual precipitation and available energy in determining annual runoff rates.

## 6. Summary and conclusions

The control of available energy and precipitation in determining annual evapotranspiration and runoff rates has been highlighted in a number of studies. Schreiber (1904), Ol'dekop (1911), Budyko (1948), Turc (1954), and Pike (1964) have successfully expressed annual evaporation ratio from catchments as a function of aridity index using different functional forms. Zhang et al. (2001) developed a new functional form using aridity index and additionally a plant-available water coefficient ($w$) which takes into account the fact that forests can transpire more water than herbaceous plants and grasses because of their deep root systems. Koster and Suarez (1999) test GCM data against Budyko's formula and extend the use of aridity index to determine evaporation deviation ratio, that is ratio of standard deviation of annual evapotranspiration values to that of precipitation.

This study evaluates the annual evapotranspiration and precipitation values from the AMIP 2 simulation made with the CCCma AGCM3 against the Schreiber, Ol'dekop, Budyko, Turc–Pike, and Zhang et al.'s functional forms. It is shown that values from CCCma AGCM3 compare well with these functional forms, and the primary control of precipitation and available energy in annual partitioning of precipitation is preserved reasonably well in the GCM. Using Koster and Suarez's (1999) equation, expressions of evaporation deviation ratio are obtained corresponding to the five functional forms and AGCM3 data are compared against these formulae. Although, the interannual variations in precipitation and potential evaporation are neglected in the expressions for evaporation deviation ratio, the $\sigma_{ET}/\sigma_P$ versus $\phi$ curves predicted by the five functional forms describe the general behavior of interannual variations in model evapotranspiration values fairly well.

Budyko's approach and the use of aridity index is extended to obtain an expression for change in annual runoff given information about changes in precipitation and potential evaporation. This expression for change in runoff is similar to the one obtained by Dooge (1992) and Dooge et al. (1999) but differs in its mathematical form since Dooge (1992) developed his expression in terms of humidity index rather than the aridity index. This expression for obtaining a first-order estimate of annual change in runoff is tested using data from control and transient enhanced greenhouse warming simulations of the CCCma's coupled GCM. The estimates of change in runoff obtained using the aridity index compare well with the CGCM1 simulated values. The correlation between

CGCM1 simulated annual runoff changes and values predicted by using aridity index is consistently around 0.95 and the average bias varies between 40.54 and 50.31 mm/year, for the five functional forms. The successful validation of the use of aridity index to obtain an estimate of change in runoff against GCM data from a climate change simulation demonstrates the strong control of available energy and precipitation in determining annual evapotranspiration and runoff rates, and the continued relevance of aridity index in analyses of Budyko and other researchers. It is also found that annual changes in runoff predicted by the five functional forms are similar to each other and no single functional form stands out as an outlier. Thus any of the five functional forms may be used to obtain an estimate of change in runoff.

The simple expression for obtaining an estimate of change in runoff based on changes in precipitation and potential evaporation, and the use of aridity index, provides a straight-forward method to obtain a first-order estimate of the effect of climate change on annual runoff with performing detailed hydrological model simulations.

## Acknowledgments

The author would like to thank the two anonymous reviewers for their constructive criticism and helpful comments.

## References

Abdella, K., McFarlane, N.A., 1996. Parameterization of the surface-layer exchange coefficients for atmospheric models, B. Layer Met. 80, 223–248.

Arora, V.K., 2001a. Assessment of simulated water balance for continental-scale river basins in an AMIP 2 simulation. J. Geophys. Res. 106 (D14), 14827–14842.

Arora, V.K., 2001b. Streamflow simulations for continental scale river basins in a global atmospheric general circulation model. Adv. Water Resour. 24 (7), 775–791.

Arora, V.K., Boer, G.J., 2000. The effects of simulated climate change on the hydrology of major river basins, CAS/JSC WGNE Research Activities in Atmospheric and Oceanic Modelling, Report No. 30, February 2000, WMO/TD No. 987, 7.1–7.2.

Arora, V.K., Boer, G.J., 2002. A GCM-based assessment of simulated global moisture budget and the role of land-surface moisture reservoirs in processing precipitation, accepted, Climate Dynamics.

Arora, V.K., Boer, G.J., 2001. Effects of simulated climate change on the hydrology of major river basins. J. Geophys. Res. 106 (D4), 3335–3348.

Avila, A., Neal, C., Terradas, J., 1996. Climate change implications for streamflow and streamwater chemistry in a Mediterranean catchment. J. Hydrol. 177, 99–116.

Boer, G.J., 1995. A hybrid moisture variable suitable for spectral GCMs, in Research Activities in Atmospheric and Oceanic Modelling, WGNE Report No. 21, WMO/TD-No. 665, World Meteorological Organisation, Geneva.

Boer, G.J., Flato, G., Reader, M.C., Ramsden, D., 2000a. A transient climate change simulation with greenhouse gas and aerosol forcing: experimental design and comparison with the instrumental record for the twentieth century. Clim. Dyn. 16 (6), 405–425.

Boer, G.J., Flato, G., Ramsden, D., 2000b. A transient climate change simulation with greenhouse gas and aerosol forcing: projected climate to the twenty-first century. Clim. Dyn. 16 (6), 427–450.

Budyko, M.I., 1948. Evaporation under natural conditions, Gidrometeorizdat, Leningrad, English translation by IPST, Jerusalem.

Budyko, M.I., 1951. On climatic factors of runoff. Prob. Fiz. Geogr. 16 in Russian.

Budyko, M.I., 1974. Climate and life, Academic Press, Orlando, FL, 508 pp..

Budyko, M.I., Zubenok, L.I., 1961. The determination of evaporation from the land surface. Izv. Ak. Nauk SSR, Se. Geog. 6, 3–17.in Russian.

Chiew, F.H.S., Whetton, P.H., McMahon, T.A., Pittock, A.B., 1995. Simulation of the impacts of climate change on runoff and soil moisture in Australian catchments. J. Hydrol. 167, 121–147.

Dooge, J.C.I., 1992. Sensitivity of runoff to climate change: a Hortonian approach. Bull. Am. Meteorol. Soc. 73 (12), 2013–2024.

Dooge, J.C.I., Bruen, M., Parmentier, B., 1999. A simple model for estimating the sensitivity of runoff to long-term changes in precipitation without a change in vegetation. Adv. Water Resour. 23, 153–163.

Fiorino, M., 1997. AMIP II sea surface temperature and sea ice concentration observations, AMIP web site, http://www-pcmdi.llnl.gov/amip/AMIP2EXPDSN/BCS_OBS/amip2_bcs.htm.

Flato, G.M., Boer, G.J., Lee, W.G., McFarlane, N.A., Ramsden, D., Reader, M.C., Weaver, A.J., 2000. The Canadian centre for climate modelling and analysis global coupled model and its climate. Clim. Dyn. 16 (6), 451–467.

Gates, L.W., Boyle, J.S., Covey, C., Dease, C.G., Doutriaux, C.M., Drach, R.S., Fiorino, M., Glecker, P.J., Hnilo, J.J., Marlais, S.M., Phillips, T.J., Potter, G.L., Santer, B.D., Sperber, K.R., Taylor, K.E., Williams, D.N., 1999. An overview of the results of the atmospheric model intercomparison project (AMIP I). Bull. Am. Met. Soc. 80(1), 29–56.

Holzer, M., 1996. Optimal spectral topography and its effect on model climate. J. Clim., 2443–2463.

Koster, R.D., Suarez, M.J., 1999. A simple framework for

examining the interannual variability of land surface moisture fluxes. J. Clim. 12, 1911–1917.

Langner, J., Rodhe, H., 1991. A global three dimensional model of the tropospheric sulphur cycle. J. Atmos. Chem. 13, 225–263.

McFarlane, N.A., Boer, G.J., Blanchet, J.-P., Lazare, M., 1992. The Canadian climate centre second-generation general circulation model and its equilibrium climate. J. Clim. 5, 1013–1044.

Milly, P.C.D., 1994. Climate, soil water storage, and the average annual water balance. Water Resour. Res. 30 (7), 2143–2156.

Mitchell, J., Johns, T.C., Gregory, J., Tett, S., 1995. Climate response to increasing levels of greenhouse gases and sulfate aerosols. Nature 376, 501–504.

Nemec, J., Schaake, J.C., 1982. Sensitivity of water resources systems to climate variations. Hydrol. Sci. J. 27, 327–343.

Ol'dekop, E.M., 1911. On evaporation from the surface of river basins. Trans. Met. Obs. lur-evskogo, Univ. Tartu 4 in Russian.

Pacanowski, R.C., Dixon, R.C., Rosati, A., 1993. The GFDL modular ocean model users guide, GFDL Ocean Group Tech. Rep. 2, Geophysical Fluid Dynamics Laboratory, Princeton, USA, 46 pp.

Pike, J.G., 1964. The estimation of annual runoff from meteorological data in a tropical climate. J. Hydrol. 2, 116–123.

Ponce, V.M., Pandey, R.P., Ercan, S., 2000. Characterization of drought across the climate spectrum. J. Hydrol. Engng, ASCE 5 (2), 222–224.

Reader, M.C., Boer, G.J., 1998. The modification of greenhouse gas warming by the direct effect of sulphate aerosols. Clim. Dyn. 14, 593–607.

Schreiber, P., 1904. Über die Beziehungen zwischen dem Niederschlag und der Wasserführung der Flüße in Mitteleuropa. Z. Meteorol. 21 (10), 441–452.

Singh, P., Kumar, N., 1997. Impact assessment of climate change on the hydrological response of a snow and glacier melt runoff dominated Himalayan river. J. Hydrol. 193, 316–350.

Turc, L., 1954. Le bilan d'eau des sols. Relation entre la précipitation, l;évaporation et l;écoulement. Ann. Agron. 5, 491–569.

Verseghy, D.L., McFarlane, N.A., Lazare, M., 1993. CLASS—a Canadian land surface scheme for GCMs: II. Vegetation model and coupled runs. Int. J. Climatol. 13, 347–370.

Zhang, G.J., McFarlane, N.A., 1995. Sensitivity of climate simulations to the parameterization of cumulus convection in the CCC GCM. Atmos.–Ocean, 407–446.

Zhang, L., Dawes, W.R., Walker, G.R., 2001. Response of mean annual evapotranspiration to vegetation changes at catchment scale. Water Resour. Res. 37 (3), 701–708.